Transactions on Engineering and Technology Research
ISSN: 2960-1797, eISSN: 2960-2246 | Volume 6
MECEME 2026

Research on the Thickness of Silicon Carbide Epitaxial Layer Based on the Geometrical Optics Propagation Model

Leqi Wang *

School of Economics and Finance, University of International Relations, Beijing, China

* Corresponding Author Email: 13269955112@163.com

Abstract. Silicon Carbide (SiC), as a third-generation semiconductor material, is widely used in electronic devices operating in extreme environments such as high temperature and high pressure. The thickness of the epitaxial layer greatly impacts the performance of SiC devices, making its precise measurement crucial. Infrared interferometry is a commonly used non-destructive measurement method, but existing studies often neglect the multi-beam interference effect. This paper proposes an improved method for measuring the epitaxial layer thickness by utilizing data from the 2025 National College Student Mathematical Modeling Competition B-topic, based on a single reflection and refraction model for calculating the epitaxial layer thickness. Data analysis confirmed the existence of multi-beam interference effects and led to the revision of the model, eliminating the impact of this effect on measurement accuracy. The corrected model improves measurement accuracy, with results significantly more accurate than traditional methods, proving the importance of multi-beam interference effects in thickness measurement. This method provides an effective solution for the precise measurement of SiC epitaxial layers and has significant practical application value.

Keywords: Silicon Carbide; Epitaxial Layer Thickness; Infrared Interferometry; Multi-beam Interference; Geometrical Optics Model.

1. Introduction

With the rapid development of information technology, Silicon Carbide (SiC), as a third-generation semiconductor material, has seen increasingly widespread applications in extreme environments such as high power, high frequency, and high temperature, particularly in fields like power electronics, automotive electronics, and 5G communication. The excellent properties of SiC, such as high breakdown voltage, high thermal conductivity, and wide bandgap, make it a core material for next-generation power electronic devices [1][2]. As the demand for high-performance SiC devices increases, the manufacturing process faces increasingly stringent requirements, especially in the control of the epitaxial layer thickness, which has become a critical factor in enhancing device performance.

Currently, infrared interferometry has become a commonly used non-destructive technique for measuring the thickness of thin films and epitaxial layers. This method is based on the interference effect of light waves, calculating the material thickness by analyzing the interference fringes between reflected and refracted light. Traditional infrared interferometry typically assumes that light waves only undergo a single reflection and transmission at the epitaxial layer surface and substrate interface, considering only the interference effect of single reflection and transmission [3][4]. However, as the epitaxial layer thickness changes and the angle of incidence of the light waves varies, light waves may undergo multiple reflections and transmissions between the epitaxial layer and the substrate, leading to complex multi-beam interference effects [5]. Most existing studies still neglect this effect, leading to insufficient measurement accuracy in some cases.

This paper proposes a new method for measuring the thickness of the SiC epitaxial layer based on infrared interferometry, introducing the analysis of multi-beam interference effects to improve the traditional measurement model, thus achieving more precise thickness measurements. This method not only provides an effective solution for the high-precision measurement of SiC epitaxial layer

Content from this work may be used under the terms of CC BY-NC 4.0 licence (https://creativecommons.org/licenses/by-nc/4.0/).
Published by Warwick Evans Publishing.

thickness but also offers important theoretical foundations and technical support for the future development of semiconductor manufacturing technology.

2. Research Methods

2.1. Data Sources and Study Design

The data used in this study come from the attachments in the 2025 National College Student Mathematical Modeling Competition B-topic. Specifically, Attachments 1 and 2 record the reflection spectrum data of SiC wafers at incident angles of 10° and 15°, respectively: wavenumber (cm^{-1}) and reflectance ($\%$). These data are used to validate the performance of the traditional model and the improved model in practical applications.

The goal of this study is to propose an improved model for measuring the thickness of SiC epitaxial layers, addressing the multi-beam interference effect that is neglected in traditional infrared interferometry. This study is divided into three main steps: first, constructing a basic model of single reflection and refraction to calculate the thickness of the SiC epitaxial layer in Attachments 1 and 2; then, analyzing whether there is a multi-beam interference effect in these data and assessing its impact on thickness calculation; finally, improving the model based on the principles of multi-beam interference and eliminating this interference effect, recalculating the epitaxial layer thickness, and comparing the two results to analyze whether multi-beam interference affects the thickness measurement results.

2.2. Establishment and Solution of Single Reflection and Refraction Models

First, this paper constructs a simple mathematical model, considering only a single reflection and transmission of light waves at the epitaxial layer surface and the substrate interface. As shown in Figure 1, the model is based on the principles of optical interference. When light waves incident on the epitaxial layer, part of the wave is reflected, forming a reflected beam, while another part transmits through the epitaxial layer, propagating after being reflected by the substrate interface. According to the basic principles of geometrical optics, the path difference of the light waves causes a phase difference, which in turn forms interference fringes.

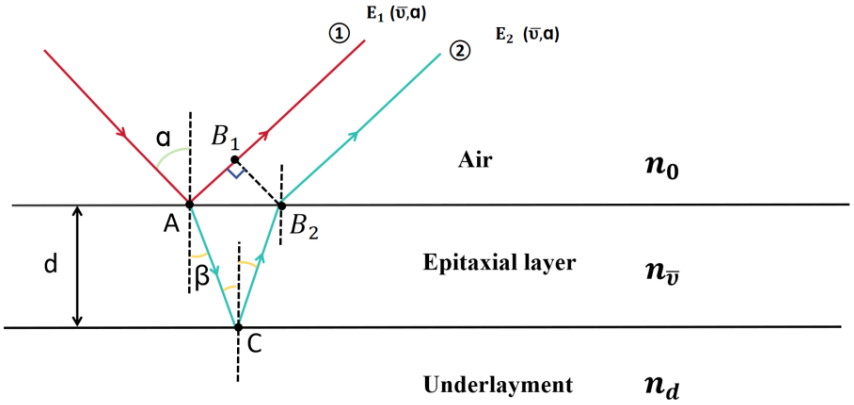

Figure 1. Schematic diagram of the principle of single reflection and refraction measurement of epitaxial layer thickness

First, by combining the wavenumber and reflectance information provided by the data, and applying the principles of physical optics and geometrical optics, the phase changes φ_1 and φ_2 of the reflected and refracted light are derived:

$$\varphi_1 = 2d \cdot \tan\beta \cdot \sin\alpha \cdot n_0 \cdot \upsilon \cdot 2\pi + r_A \tag{1}$$

$$\varphi_2 = \frac{2d}{\cos\beta} \cdot n_\upsilon \cdot \upsilon \cdot 2\pi + r_C \tag{2}$$

According to the basic principles of interference light, the amplitude of the reflected and refracted light is superimposed, and combining the definition of light intensity with the intensity expression of the interference light:

$$E\cos(2\pi\upsilon x + \varphi_0) = E_1\cos(2\pi\upsilon x + \varphi_1) + E_2\cos(2\pi\upsilon x + \varphi_2) \tag{3}$$

$$I = E^2 = {E_1}^2 + {E_2}^2 + 2E_1E_2\cos(\varphi_2 - \varphi_1) \tag{4}$$

Where I represents the intensity of the interference light; E represents the amplitude of the interference light; φ_0 is the initial phase of the interference light; and $\cos(\varphi_2 - \varphi_1)$ is the interference term caused by the phase difference between the reflected and refracted light.

Finally, the function relationship between reflectance γ and wavenumber υ is derived:

$$\gamma = \frac{{E_1}^2 + {E_2}^2 + 2E_1E_2\cos[2d(\frac{n_\upsilon}{\cos\beta} - \tan\beta\sin\alpha)\upsilon \cdot 2\pi + (r_C - r_A)]}{{E_0}^2} \tag{5}$$

Where E_1 represents the amplitude of the reflected light, E_2 represents the amplitude of the refracted light, d represents the epitaxial layer thickness, n_υ represents the refractive index of the epitaxial layer (assumed to be a constant of 2.55 in this paper [5]), α represents the angle of incidence, β represents the angle of refraction, r_A represents the half-wave loss of the reflected light, r_C represents the half-wave loss of the refracted light, and E_0 represents the amplitude of the incident light.

By appropriately rearranging the above model, we get:

$$\gamma = \frac{{E_1}^2 + {E_2}^2}{{E_0}^2} + \frac{2E_1E_2}{{E_0}^2} \cdot \cos[(\frac{n_\upsilon}{\cos\beta} - \tan\beta\sin\alpha n_0) \cdot 4\pi \cdot d \cdot \upsilon + r_0] \tag{6}$$

Where: Let

$$\begin{cases} \theta_{1(\upsilon)} = \dfrac{{E_1}^2 + {E_2}^2}{{E_0}^2} \\ \theta_{2(\upsilon)} = \dfrac{2E_1E_2}{{E_0}^2} \\ \theta_{3(\upsilon)} = (\dfrac{n_\upsilon}{\cos\beta} - \tan\beta\sin\alpha n_0) \cdot 4\pi \cdot d \end{cases} \tag{7}$$

We get:

$$\gamma = \theta_{1(\upsilon)} + \theta_{2(\upsilon)} \cdot \cos[\theta_{3(\upsilon)} \cdot \upsilon + r_0] \tag{8}$$

Where $\theta_{1(\upsilon)}$ is a smooth function representing the basic trend between reflectance and wavenumber; $\theta_{2(\upsilon)} \cdot \cos[\theta_{3(\upsilon)} \cdot \upsilon + r_0]$ is the periodic variation part, which represents the interference component of reflectance changes.

First, this paper uses scatter plots to visualize the wavenumber and reflectance data provided in Attachments 1 and 2, resulting in Figure 2 and Figure 3. Through these data, the trends can be intuitively observed, leading to the γ function.

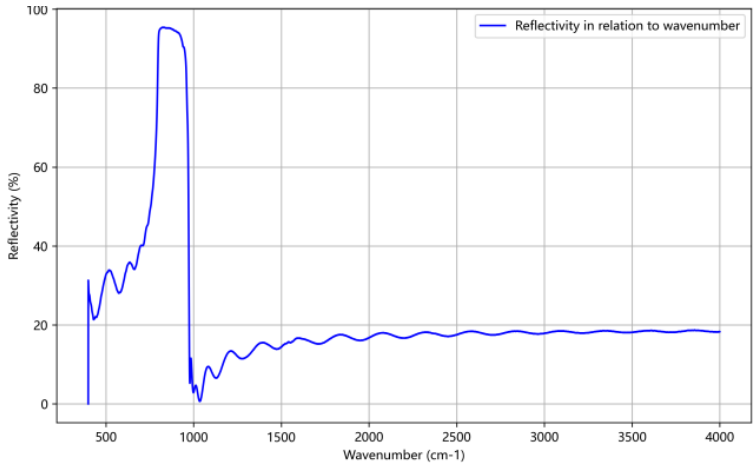

Figure 2. Wavenumber and reflectance relationship graph in Attachment 1 (α=10°)

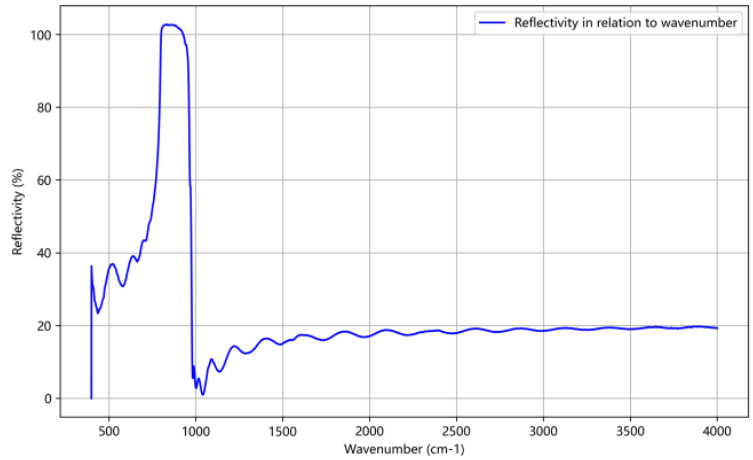

Figure 3. Wavenumber and reflectance relationship graph in Attachment 2 (α=15°)

Subsequently, the paper applies Gaussian filtering to smooth the γ function, resulting in $\theta_{1(\upsilon)}$. Gaussian filtering is a commonly used smoothing method that removes noise from images or signals while retaining the main features of the data. It achieves the smoothing effect by convolving the Gaussian function with the data.

Through literature review, the paper found that due to the Reststrahlen band in crystalline materials, i.e., the optical phonon resonance effect, total reflection occurs between transverse and longitudinal optical phonon frequencies at the interface. However, reflectance drops significantly after passing through the band [6]. Therefore, the data in the 800-1500 wavenumber range are unsuitable for thickness measurement and are discarded based on physical principles.

As shown in Figure 2 and Figure 3, the data exhibits significant oscillation. To improve the accuracy of the d values, piecewise smoothing is applied with a segment size of 300 wavenumbers. Due to the large number of segments, only the results for the wavenumber ranges 1700-2000 and 3500-3800 are shown below.

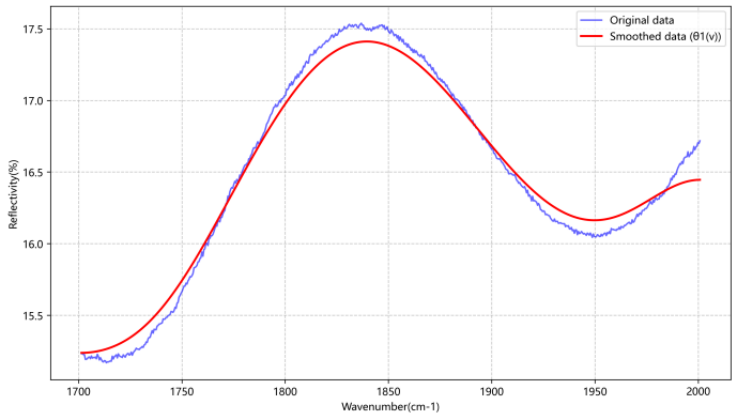

Figure 4. $\gamma - \upsilon$ plot for Attachment 1 (1700-2000)

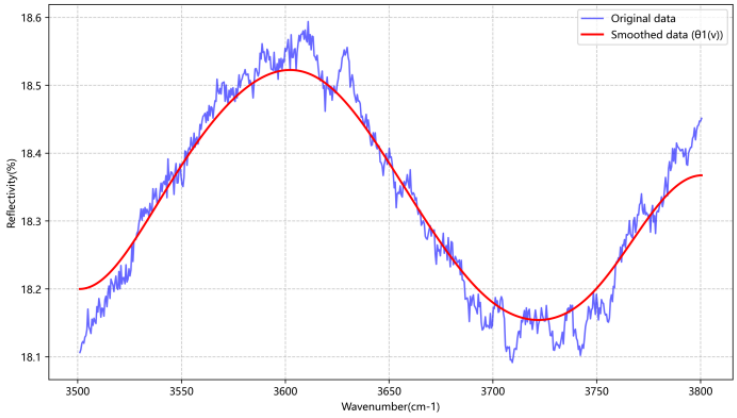

Figure 5. $\gamma - \upsilon$ plot for Attachment 1 (3500-3800)

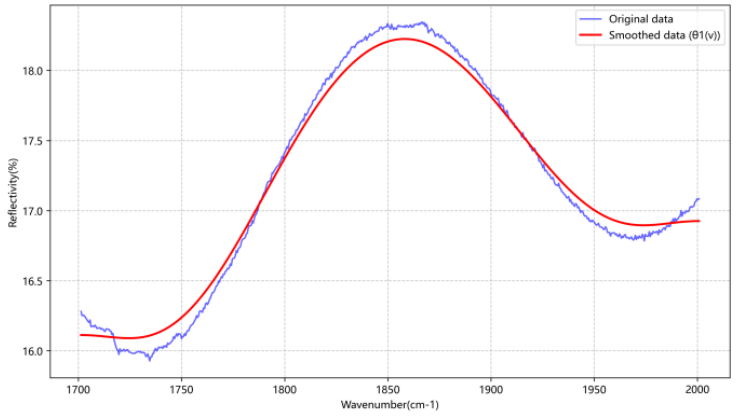

Figure 6. $\gamma - \upsilon$ plot for Attachment 2 (1700-2000)

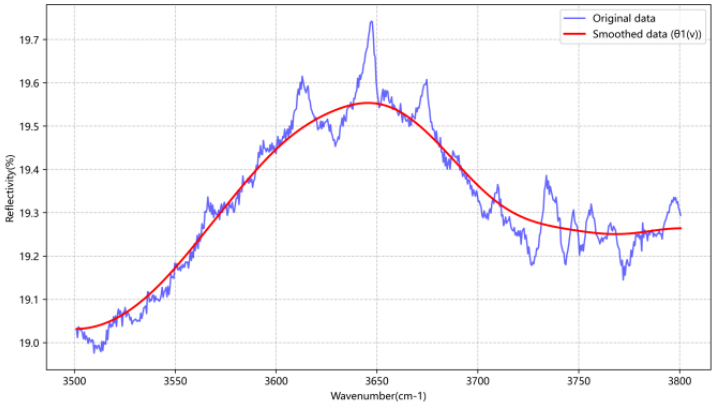

Figure 7. $\gamma - \upsilon$ plot for Attachment 2 (3500-3800)

Figure 4 and Figure 5 show the comparison between the original data and the smoothed data within two different wavenumber ranges (1700-2000 and 3500-3800) in Attachment 1. In Figure 4, the smoothed data (in red) clearly smoothes out the oscillations in the original data (in blue), displaying the variation trend within the 1700-2000 wavenumber range. Similarly, Figure 5 also shows the measurement data in the 3500-3800 wavenumber range, where the smoothed data exhibits significantly reduced fluctuations compared to the original data, making it more stable. These plots clearly illustrate the effect of Gaussian filtering on smoothing the data, providing more accurate input for further thickness measurements.

Figure 6 and Figure 7 continue to show the smoothing effects of the data for Attachment 2 in different wavenumber ranges. Figure 6 focuses on the 1700-2000 wavenumber range, where the smoothed data eliminates noise from the original data, optimizing the reliability of the data. Figure 7 shows the data processing results in the 3500-3800 wavenumber range, further verifying the importance of smoothing in reducing measurement errors and improving data accuracy. These improvements will directly impact the accuracy and precision of the subsequent epitaxial layer thickness calculations.

Next, the nonlinear least squares method is used to fit the interference component $\theta_{2(\upsilon)} \cdot \cos[\theta_{3(\upsilon)} \cdot \upsilon + r_0]$. By outputting the parameter values, the unknown parameters ($\theta_{2(\upsilon)}, \theta_{3(\upsilon)}, r_0$) can be solved.

The final thickness d output result is:

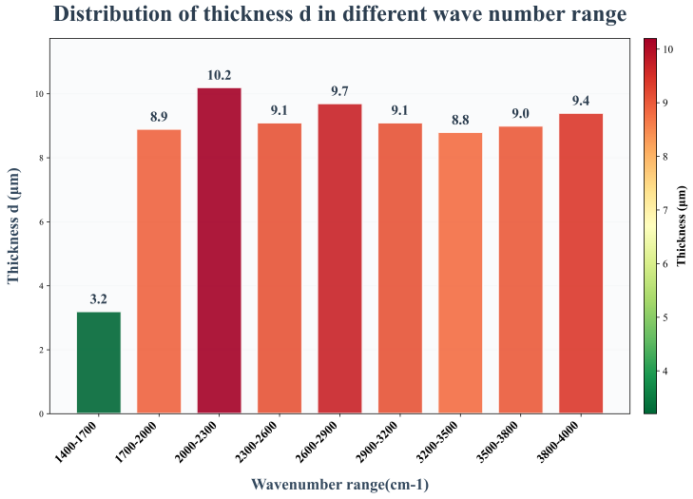

Figure 8. Thickness d distribution in different wavenumber ranges for Attachment 1

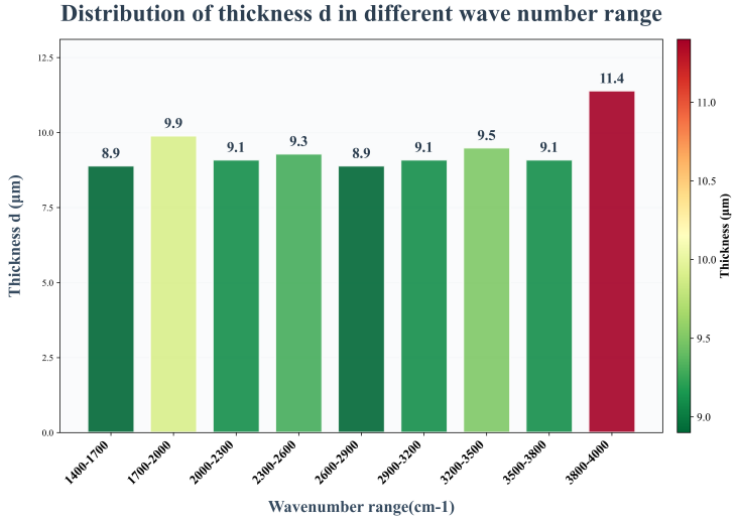

Figure 9. Thickness d distribution in different wavenumber ranges for Attachment 2

From the thickness distribution in different wavenumber ranges shown in Figure 8 and Figure 9, it can be observed that the epitaxial layer thickness varies significantly across different wavenumber ranges. Specifically, in Attachment 1 (Figure 8), the thickness in the 1700-2000 wavenumber range is noticeably smaller (3.2 μm), while the thickness in other wavenumber ranges is significantly larger, especially in the 2000-2300 wavenumber range, where the thickness reaches 10.2 μm . This variation is likely closely related to the multi-beam interference effect. In the higher wavenumber ranges, light waves may undergo multiple reflections and transmissions between the epitaxial layer and the substrate, which leads to changes in the interference fringes, thus affecting the thickness measurement results.

In Figure 9 (Attachment 2), although the thickness distribution across different wavenumber ranges is relatively stable, it can still be observed that the highest thickness (11.4 μm) appears in the high wavenumber range (3800-4000). This suggests that, at larger incident angles, the reflection and transmission effects of light waves in the higher wavenumber range are more pronounced, potentially triggering multi-beam interference, which has a more significant impact on thickness measurements, leading to larger variations in thickness values.

These observations indicate that the multi-beam interference effect may cause deviations in thickness measurement, especially in higher wavenumber ranges and at larger incident angles. The interference effect significantly influences the measurement accuracy of the epitaxial layer thickness. Therefore, by correcting the measurement model to account for the multi-beam interference effect, the measurement accuracy can be improved, eliminating errors introduced by the interference effect.

The results from Figure 8 and Figure 9 are summarized in Table 1 and Table 2:

Table 1. Attachment 1 *d* Calculation Results Table

Wavenumber range	1400-4000 cm^{-1}
Thickness range	8.9-11.4 μm
Average thickness	9.5 μm
Maximum thickness	11.4 μm
Minimum thickness	8.9 μm

Table 2. Attachment 2 *d* Calculation Results Table

Wavenumber range	1400-4000 cm^{-1}
Thickness range	8.8-10.2 μm
Average thickness	9.2 μm
Maximum thickness	10.2 μm
Minimum thickness	8.8 μm

Table 1 and Table 2 show the calculation results of the SiC epitaxial layer thickness for different incident angles. Table 1 lists the thickness range, average thickness, maximum thickness, and minimum thickness of the epitaxial layer in Attachment 1 (wavenumber range: 1400-4000 cm^{-1}). According to the table, the thickness range is from 8.9 μm to 11.4 μm , with an average thickness of 9.5 μm , a maximum thickness of 11.4 μm , and a minimum thickness of 8.9 μm . These results indicate that, within this wavenumber range, the epitaxial layer thickness shows significant variation, and the higher the wavenumber range, the more pronounced the thickness fluctuations.

Table 2 presents the calculation results for Attachment 2 (wavenumber range: 1400-4000 cm^{-1}). The thickness range is from 8.8 μm to 10.2 μm, with an average thickness of 9.2 μm, a maximum thickness of 10.2 μm, and a minimum thickness of 8.8 μm. Compared to Table 1, the thickness range and fluctuations in Table 2 are relatively smaller, indicating that the epitaxial layer thickness variation is more stable in this wavenumber range.

From the results of these two tables, it can be seen that the epitaxial layer thickness exhibits different trends and fluctuations depending on the wavenumber range. The higher wavenumber ranges (as shown in Table 1) lead to greater thickness variations, while the lower wavenumber ranges (as shown in Table 2) present relatively more stable thickness changes. These data provide important insights into the thickness characteristics of the epitaxial layer and further confirm the impact of the multi-beam interference effect on measurement accuracy in high wavenumber ranges.

2.3. Analysis of Multi-Beam Interference Effects

Using the model constructed above, the epitaxial layer thickness was calculated based on infrared interferometry under single reflection and transmission conditions. However, with varying angles of incidence and changes in the epitaxial layer thickness, as shown in Figure 10, light waves may undergo multiple reflections and transmissions between the epitaxial layer and substrate, leading to complex multi-beam interference effects. According to research by Zhu Hongyu and others, multi-beam interference arises from the phase differences of multiple interference beams generated by light waves reflecting at different interfaces. At larger incident angles, such as 15°, the reflectance of the light waves is higher, which increases the number of reflections and transmissions between the epitaxial layer and the substrate, thereby triggering multi-beam interference [7].

In comparison to single reflection, multiple reflections and transmissions of light waves between the epitaxial layer and the substrate create more complex phase differences. To address this issue, this paper further analyzed whether multi-beam interference effects exist in the data. The result showed that at an incident angle of 15° and a wavenumber of 400.1569 cm^{-1}, a significant change in reflectance occurred, indicating that multi-beam interference may arise at this angle.

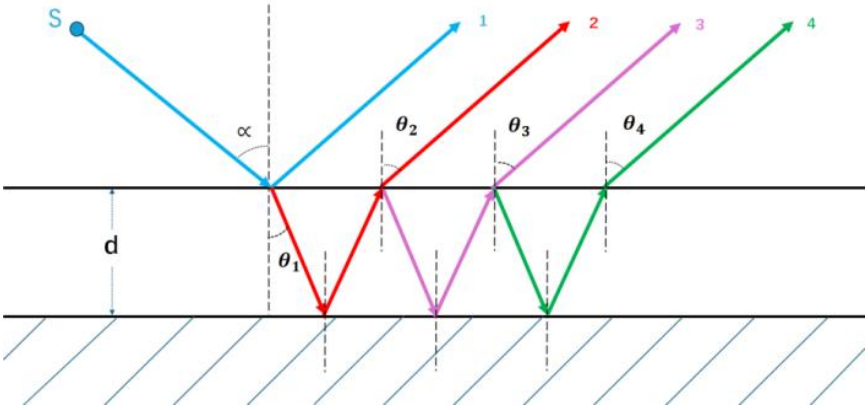

Figure 10. Multi-Beam Interference Principle Diagram

2.4. Correction of the Multi-Beam Interference Model

For the multi-beam interference phenomenon, the intensity of the interference light depends not only on the phase difference between the single reflected and refracted light, but is also determined by the phase differences of all reflected and refracted light beams. Therefore, for multi-beam interference to occur, the phase differences between all reflected and refracted light beams must satisfy the interference conditions. Specifically, the phase difference of the light waves should meet the following condition:

$$\Delta\varphi_n = m_n \cdot 2\pi \qquad \text{(Constructive Interference)} \qquad (9)$$

Or

$$\Delta\varphi_n = (m_n + \frac{1}{2}) \cdot 2\pi \quad \text{(Destructive Interference)} \tag{10}$$

Where m_n is an integer, representing that constructive interference occurs when the phase difference between different reflected light beams is an integer multiple of the wavelength, while destructive interference occurs when the phase difference is an odd multiple of half the wavelength.

To ensure the occurrence of multi-beam interference effects, the phase difference between each reflected and refracted light beam must satisfy the above relationship. In other words, the light waves along different paths must meet the condition that the phase difference is an integer multiple of 2π, or an odd multiple of half the wavelength, to produce the interference effect.

After explaining the conditions for the occurrence of multi-beam interference, to address the thickness measurement errors caused by the multi-beam interference effect, this paper modifies the traditional model. By considering the paths of multiple reflected light beams, the expression for the interference light intensity I is derived:

$$I = (E_1 + E_2 + \cdots + E_n)^2 = \sum_{i=1}^{n} E_i^2 + 2\sum_{i<j} E_i E_j \cos(\Delta\varphi_{ij}) \tag{11}$$

Where E_1 is the amplitude of the i light beam, and $\Delta\varphi_{ij}$ is the phase difference between the i and j light beams. Due to the interference effects of multiple beams, the relationship between reflectance and wavenumber becomes more complex. In this paper, these interference terms are solved through fitting.

After confirming the influence of the multi-beam interference effect, this paper further improves the original model and derives the new epitaxial layer thickness calculation formula:

$$\gamma = \frac{A \cdot \cos^2[\frac{2\pi d}{\lambda}\cos(\alpha)]}{1 + B \cdot \cos^2[\frac{2\pi d}{\lambda}\cos(\alpha)]} \tag{12}$$

Where γ is the reflectance, A and B are fitting parameters, λ is the wavelength, and α is the angle of incidence.

To eliminate the impact of multi-beam interference on measurement accuracy, this model uses Gaussian filtering to smooth the data, thereby removing the noise from the reflected light and enhancing the clarity of the interference fringes. Then, the nonlinear least squares method is used to fit the interference data, effectively correcting the epitaxial layer thickness calculation results and eliminating the impact of multi-beam interference.

Based on the results output from the code, the corrected epitaxial layer thicknesses for Attachment 1 and Attachment 2 are accurately calculated.

The corrected epitaxial layer thickness for Attachment 1 is $d = 8.11157\ \mu m$.

The corrected epitaxial layer thickness for Attachment 2 is $d = 5.29123\ \mu m$.

Through this correction method, the impact of interference effects on the epitaxial layer thickness measurement has been effectively eliminated.

3. Results and Discussion

In this paper, the traditional single reflection and refraction model was first used to calculate the SiC epitaxial layer thickness provided in Attachments 1 and 2. Based on the traditional model, the calculated epitaxial layer thicknesses were: 9.5 μm for Attachment 1 (incident angle 10°) and 9.2 μm for Attachment 2 (incident angle 15°). However, considering the influence of multi-beam interference effects, this paper proposes an improved model and corrects the calculation results.

In the corrected model, the multiple reflection and transmission effects that light waves may undergo between the epitaxial layer and substrate were considered. Data was smoothed using Gaussian filtering, and the nonlinear least squares method was used to fit the interference part. The final new epitaxial layer thickness values obtained were: 8.11157 μm for Attachment 1 (incident angle 10°) and 5.29123 μm for Attachment 2 (incident angle 15°). Compared to the traditional model, the corrected results significantly reduced the errors caused by interference effects, showing higher precision.

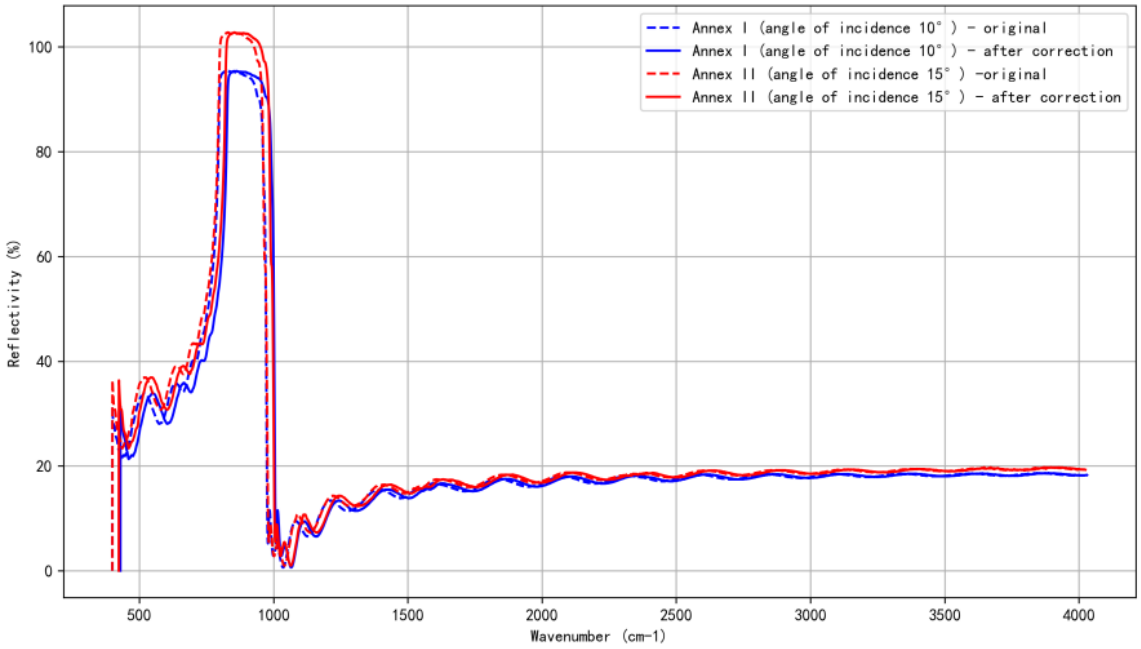

Figure 11. Reflectance vs. Wavenumber Relationship (Before and After Considering Multi-Beam Interference)

Figure 11 shows the relationship between reflectance and wavenumber for Attachments 1 and 2, with the peaks of the interference fringes marked. From the figure, it can be observed that after considering multi-beam interference, the interference fringes in reflectance have shifted slightly. This change indicates that when the multi-beam interference effect is taken into account, the position of the interference fringes shifts, which in turn affects the calculation results for the epitaxial layer thickness. This phenomenon is particularly noticeable in the reflectance data for Attachment 2 (incident angle 15°), suggesting that at larger incident angles, the impact of multi-beam interference on the measurement results is more pronounced.

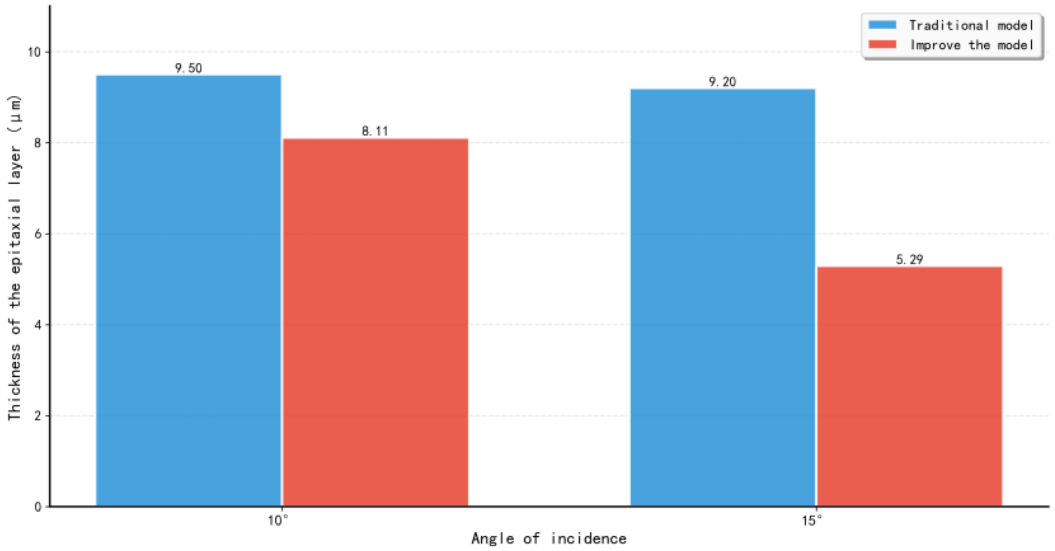

Figure 12. Comparison of Epitaxial Layer Thicknesses Between the Traditional Model and the Improved Model at Different Incident Angles

Figure 12 compares the epitaxial layer thicknesses calculated by the traditional model and the improved model at different incident angles. In the figure, it can be seen that there is a noticeable difference in the thickness calculation results between the traditional model (which neglects the multi-beam interference effect) and the improved model, especially at an incident angle of 15°. Specifically, the thickness calculated by the traditional model is overestimated, while the improved model fits the experimental data more accurately, reducing the errors caused by interference effects and providing more precise measurement results.

Further analysis of the data reveals that, in Attachment 2 (incident angle 15°), the reflectance fluctuates significantly at multiple wavenumber points, particularly at a wavenumber of $400.1569\,cm^{-1}$, where the reflectance variation is especially sharp. According to the research by Zhu Hongyu and others, the multi-beam interference effect is more pronounced at large incident angles (such as 15°) [8-12], which is also confirmed by the experimental data. This paper further analyzes and confirms this phenomenon and eliminates its impact on the epitaxial layer thickness measurement through the corrected model.

4. Conclusion

This paper proposes an improved method for measuring the thickness of silicon carbide (SiC) epitaxial layers, addressing the multi-beam interference effect that is ignored in traditional infrared interferometry. By constructing and optimizing the mathematical model, the thickness of the epitaxial layer is first calculated using a single reflection and refraction model, followed by the introduction of the multi-beam interference effect and model correction. The calculation results show that the traditional model, due to the neglect of the multi-beam interference effect, generally overestimates the measurement values and introduces certain errors, while the corrected model effectively eliminates these errors, providing more accurate measurement results.

By incorporating the analysis of the multi-beam interference effect and using Gaussian filtering to smooth the data, this paper significantly improves the accuracy of the SiC epitaxial layer thickness measurement. Compared to existing measurement methods, the proposed model better accommodates the measurement requirements across different incident angles and wavenumber ranges, reducing the errors caused by interference effects that were not considered in traditional methods.

The innovation of this paper lies in successfully addressing the impact of multi-beam interference on thickness measurement accuracy through an improved mathematical model and data processing method in traditional infrared interferometry. The study demonstrates that this improved method is

not only applicable to the measurement of SiC epitaxial layer thickness, but also provides theoretical foundations and technical support for the measurement of thickness in other semiconductor materials. In the future, further experimental validation and broader application cases will help enhance the universality and accuracy of this method, offering stronger technical support for the quality control and device optimization of semiconductor materials.

Reference

[1] Tan Bingyuan, Guo Jiang, Yao Dongfang, et al. Optimization of the Manufacturing of Silicon Carbide, a Key Semiconductor Material for 5G Communication Technology in Intelligent Measurement Devices [J]. Journal of Wuhan University of Technology (Engineering Edition), 2024, 57(09): 1335-1341.

[2] Qin Xiao. Domestic Silicon Carbide Semiconductors Are Rising Across the Board [N]. China Business News, 2025-09-15(C01).

[3] Zhao Yuanyuan, Xiao Zuojiang, Liang Xu. Measurement method of glass thickness and refractive index based on spectral interference technology[J]. Infrared and Laser Engineering, 2020, 49(2): 248-253.

[4] Chong He, Yuxin Zhou, Jinjie Liu, et al. Oil film measurement method based on combination of capacitance method and optical interference method[J]. Lubrication Engineering (0254-0150), 2023, 48(2).

[5] Gao Ruibo, Ye Hansheng, Fan Wei, et al. Film Thickness Measurement Method Combining Frequency Domain White Light Interference and Reflection Spectroscopy[J]. Laser & Optoelectronics Progress, 2025, 62(3): 167-175.

[6] National Market Supervision Administration. Testing of Silicon Carbide Epitaxial Layer Thickness Using Infrared Reflection Method: GB/T 42905-2023 [S]. 2023.

[7] Tang Yulong. Surface Phonon-Polariton Excitation on Silicon Carbide [D]. Shanghai Normal University, 2017.

[8] Zhu Hongyu, Wang Qing, Xu Hang. Error Control in Small Gap Phase Shift Measurements [J]. Optical Technology, 2025, 51(01): 123-128.

[9] FAW Jiefang Automobile Co., Ltd. Testing method for film thickness: CN 202410368308.5[P]. 2024-05-28.

[10] Yang Jiwei, Dong Ling, Gu Dong, et al. Thickness Dependence Study on Infrared and Visible Light Compatible Stealth of Transparent Conductive Films[J]. Journal of Synthetic Crystals, 2025, 54(9).

[11] Zhang Youcheng, Zheng Donghui, Huang Yifei, et al. Long-Wave Infrared Interferometer Applied to Gradient Refractive Index Measurement[J]. Optical Technique, 2025, 51(2): 169-174.

[12] Wang Yating, Kong Ming, Hua Hangbo, et al. Glass Thickness Measurement Method Based on Laser Swept-Frequency Interference Ranging System[J]. Applied Laser, 2024, 44(7): 120-126.